Toward cancer characterization using light backscattering spectroscopy and quantitative ultrasound

Cyril Malinet, Pauline Muleki-Seya, Aurélie Dutour, Iveta Fajnorova, Herve Liebgott, Bruno Montcel

Toward cancer characterization using light backscattering spectroscopy and quantitative ultrasound

Cyril Malinet[⋆], Pauline Muleki-Seya[⋆], Aurélie Dutour[†], Iveta Fajnorova[†], Hervé Liebgott[⋆], and Bruno Montcel[⋆]

[⋆]Université de Lyon, CREATIS, CNRS UMR 5220, Inserm U1044, INSA-Lyon, Université Lyon 1, Lyon, France
[†]Centre de Recherche en Cancérologie de Lyon/Centre Léon Bérard, Equipe mort cellulaire et cancers pédiatriques, UMR INSERM 1052, CNRS 5286, France

ABSTRACT

Two optical techniques and two ultrasound methods have been applied on an excised mouse tumor with the aim of estimating its microstructural properties. Enhanced Backscattering Spectroscopy, Light Scattering Spectroscopy, ultrasound Backscatter Coefficient parametrization and Envelope Statistics have been performed the same day on this biological sample. Thus, different quantitative light-based and ultrasound-based parameters that reflects the scattering properties have been estimated. Histological analyses were carried out to obtain morphological information about the cell structures. The scatterer size distribution extracted by the Backscatter Coefficient parametrization (mean radius = 9.2 μm) overestimates the cell size (mean radius = 4.6 μm). However, a good agreement have been observed between the experimental data and the models for Enhanced Backscattering Spectroscopy and Envelope Statistics (respectively $R^2 = 0.98$, $R^2_{env,HK} = 0.98 \pm 0.01$ and $R^2_{env,Nak} = 0.90 \pm 0.03$). These two techniques brought quantitative parameters with difficult absolute value interpretations. Nonetheless, they could be of prime interest in studies with different type of tissue for classification purposes.

Keywords: Cancer characterization, Bimodal, Enhanced backscattering spectroscopy, Light scattering spectroscopy, Backscatter coefficient, Envelope statistics

1. INTRODUCTION

Histo-cytopathology is the gold standard for diagnosing cancers. However, this method is inherently invasive. To avoid false negative biopsies, a tool able to characterize tissues in a non-invasive fashion during the surgery would be of great benefits. As a first step toward this goal, an optical and ultrasound bimodal technique has been developed. Enhanced Backscattering Spectroscopy (EBS) and Light Scattering Spectroscopy (LSS) are two quantitative light-based techniques which can be performed with the same experimental setup to characterize biological tissues.[1,2] Similarly, the Backscatter Coefficient (BSC) parametrization and the Envelope Statistics (ES) are two quantitative ultrasound techniques that can extract tissue scattering properties from the same acquisition.[3,4] Given the different wavelength ranges for each modality, one can expect the scattering process to originate from cell structures of different sizes by combining light and ultrasound. In the same note, biological samples also contain structures that span a wide range of materials. Consequently, these entities can appear as various sources of scattering due to the refractive index changes or the variations in the impedance contrast they induce. Thus, this bimodal technique has the potential to bring complementary information about the scattering structures in the probed tissue.

Light Scattering Spectroscopy (LSS) relies on the spectral analysis of the single scattering component of light. This technique aims to estimate the scatterer properties based on the spectrum shape. A successful application of LSS for detecting esophageal dysplastic sites can be found here.[2] The experimental setup for EBS is similar to the one used for LSS. EBS aims to determine the scattering parameters which shapes the phase function

Author information:
Cyril Malinet: E-mail: cyril.malinet@creatis.insa-lyon.fr, Telephone: +33 (0)4 72 43 74 55
Bruno Montcel: E-mail: bruno.montcel@creatis.insa-lyon.fr, Telephone: +33 (0)4 72 44 84 36

by analyzing the tissue spatial reflectance profile. Numerous studies have investigated the ability of EBS for detecting ultrastructural alterations in the field carcinogenesis.[5–7]

Conventional B-mode images bring anatomical information and are generated from radio-frequency (RF) signals backscattered from the tissue. However, the RF signals can also reveal much more information data when the spectral content is analysed (e.g. BSC parametrization) or when the statistics of the envelope is studied (Envelope Statistics). These techniques aim to extract quantitative parameters from the probed tissue. For instance, multiparametric studies can combine BSC parametrization and ES to classify cancer type[3]

In a first step, the double experimental setup for EBS and BSC parametrization has been validated on three tissue-mimicking phantoms which consisted in suspended microparticles of different sizes.[8] A certain complementarity has been observed between the two techniques regarding the sensitivity to the scatterer size. This led us to investigate the performances in characterizing an osteosarcoma from a mouse tibia with histological examinations as ground truths. In this study, we also used ES and LSS as complementary tools for this purpose. After the description of each method, the results are analysed. Last, the performances of each technique are discussed.

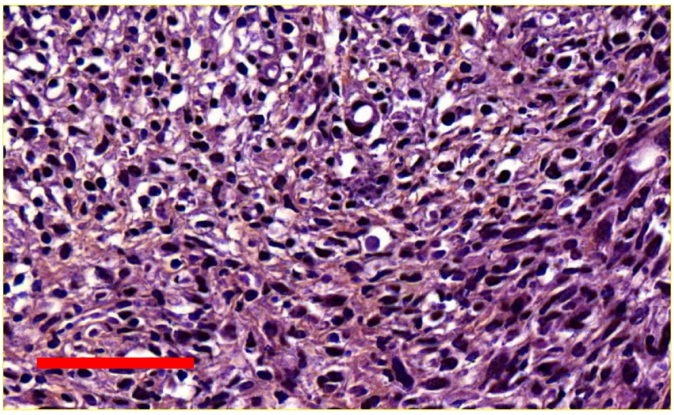

Figure 1. Osteosarcoma histological slice (HPS stain, scale bar = 20µm)

2. MATERIALS AND METHODS

2.1 Excised tumor

This *ex vivo* experiment was conducted in agreement with the European and French regulations and was approved by the ACCESS ethical committee. Experiments were conducted on one osteosarcoma that was surgically removed from the euthanized mouse. Briefly, the osteosarcoma model was established on anesthetized animals by injection of 1×10^6 K7M2 suspended cells. Tumor progression was monitored twice a week by palpation and caliper measurements until it reached a $500 - 600\ mm^3$ volume. The animal was then euthanized and the tumor removed for optical and ultrasound imaging, which were performed the same day. The sample was decalcified, embedded in paraffin and submitted to H&E staining before being scanned. Histological slices were analysed with Qupath (software version 0.3.2) to estimate the cell and the nucleus size distributions. An example of histological image is shown in Figure 1 and gives an insight of the tumor cellularity, the cell shapes and the nucleus sizes.

2.2 Optical experimental setup

Figure 2 illustrates the experimental setup used for EBS and LSS. A collimated beam from a broadband laser source (WhiteLase micro Compact Supercontinuum, Fianium) irradiates the excised tissue with plane waves. An iris diaphragm shaped the beam into a circular spot of 2 mm diameter to satisfy the Nyquist sampling criterion.[1] The polarizer forced the incident illumination into a vertical linear polarization. The sample was submerged in an aqueous solution of glycerol with a refractive index close to the assumed tissue refractive index (n = 1.38). The sample was gently rotated to eliminate speckle noise. The analyser was parallel to the polariser to select the

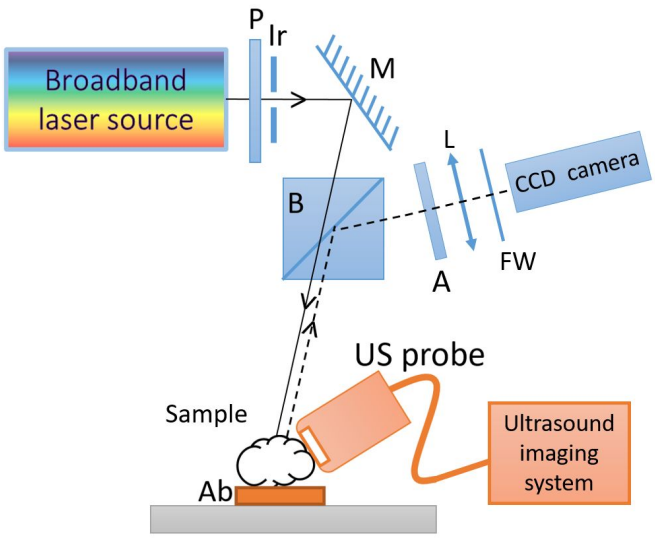

Figure 2. Experimental setup; P: polarizer, Ir: iris diaphragm, M: mirror, B: beamsplitter, A: analyzer, L: Fourier lens, FW: filter wheel, Ab: absorbing material. The detection block can be substituted by an hyperspectral camera (HERA, Nireos) for Light Scattering Spectroscopy.

copolarized channel for EBS. The camera (Thorlabs, 340M-GE) then detected the backscattered light filtered at 700 nm. The detection block (A, L, FW and CCD camera) was substituted by an hyperspectral camera (HERA, Nireos) for LSS. The exposition time was set to allow signal amplitude to reach approximately 80% of the saturation level. Each image was averaged ten times and was background-substracted.

2.3 Enhanced backscattering Spectroscopy (EBS)

The tissue reflectance profile $p(r)$ corresponds to its backscattering impulse-response, r being the exit radius of the backscattered photons. Past papers have shown that $p(r)$ is extremely sensitive to the phase function in the subdiffusion regime ($r < l_s^*$, l_s^* being the transport mean free path).[1,6] Under the approximation of a semi-infinite medium irradiated by plane waves, the reflectance profile is simply the inverse Fourier transform of the EBS peak. The EBS peak is an angular intensity peak in the exact backscattering direction that results from constructive interferences between all the time-reversed path-pairs photons. Experimentally, the CCD camera in Figure 2 images the EBS peak I_{EBS}. The latter gives access to the effective reflectance profile $p_{eff}(r)$ which represents the modulation of $p(r)$ by other functions:

$$I_{EBS}(\theta_x, \theta_y) = FT\{p_{eff}(x_s, y_s)\} = FT\{p(x_s, y_s) \cdot pc(x_s, y_s) \cdot s(x_s, y_s) \cdot c(x_s, y_s) \cdot mtf(x_s, y_s)\} \quad (1)$$

where FT denotes the 2D Fourier transform, x_s and y_s the Cartesian coordinates associated with r, pc the phase correlation function, s a modulation due to finite illumination spot size, c the spatial coherence function and mtf the imaging system's modulation transfer function. To avoid the deconvolution process and the resulting noise amplification, previous papers have shown that it is easier to fit directly $p_{eff}(r)$.[1,6] This solution requires the estimation of the modulation functions shown in Eq.1 in addition to the model for describing $p(x_s, y_s)$
The Mie theory can be helpful to describe the scattering properties from suspended microparticles[1,8] but tissue complexities can make its application difficult for biological samples. As opposed to discrete scatterers in a surrounding medium, another approach models tissues as continuous random media. Under this assumption, a versatile model that is based on the three-parameter Whittle–Matérn function to describe the refractive index correlation function can be used.[9] In this case, EBS can extract the parameters of the previous function: the characteristic length of heterogeneity of refractive index L_n, the fluctuation strength A_n and D, a parameter which determines the shape of the distribution. Radosevich et al.[6] provided a Matlab routine able to perform inversion procedures from experimental reflectance profiles to extract L_n, A_n and D.

2.4 Light Scattering Spectroscopy (LSS)

LSS aims to analyze the elastically single scattered photons to diagnose precancerous conditions. A polarization technique allows to select the differential polarization signal $\Delta I(\lambda)$, which is obtained by substracting the copolarized signal (A and P ||) with the crosspolarized signal (A and P $\perp$) after correcting for the source heterogeneities.[10] LSS models the detected spectrum as the incoherent sum of the contributions of each scatterer.[2]

$$\Delta I(\lambda) = \int_{\delta_R}^{\delta_{max}} \tilde{I}(\lambda, \delta) F(\delta)\, d\delta + \frac{C_R}{\lambda^4} + \epsilon(\lambda) \tag{2}$$

where $\tilde{I}(\lambda, \delta)$ is the LSS spectrum of a single scatterer of diameter δ, δ_R the diameter threshold below which Rayleigh scattering is considered as dominant (typically 100 nm), δ_{max} the maximum scatterer diameter, $F(\delta)$ the scatterer size distribution, C_R an unknown constant proportional to the number of Rayleigh scatterers and $\epsilon(\lambda)$ the experimental noise. Fang et al.[11] describes the analytic procedure to extract $F(\delta)$. The intensity $\tilde{I}(\lambda, \delta)$ can be computed using the Mie theory with the Python module *miepython*. Experimentally, $\Delta I(\lambda)$ was measured over the range 550-700 nm with 32 spectral points with a hyperspectral camera. To exclude coherent signal from the center, the angular intensity within a ring 0.5° and 0.85° was summed for each wavelength.

2.5 Ultrasound measurements

The sample was insonified with focused waves using two linear probes (MS250S, LZ400, Vevo) centered at 21 MHz and 30 MHz, allowing tissue characterizations over the 13 MHz - 38 MHz frequency range. A 3D scan was performed and consisted in 10 B-mode images spaced out 0.1 mm away from each other. Each scan was composed of 1536 RF lines and imaged the tumour over 15 mm in the lateral direction. Twenty three Regions of Interest (ROI) that were 15λ long in both directions located at a relatively shallow depth, were selected. The sample attenuation was estimated using a standard substitution method.[12]

2.5.1 BSC parametrization

The BSC represents the tissue ability to backscatter the acoustic energy as a function of frequency. This quantity is related to the underlying tissue structure and can be seen as the ultrasonic tissue signature.[13] The BSC for each ROI was estimated using the reference phantom method.[14] Then, the BSC estimations from each frame were averaged for the MS250S probe and the LZ400 probe (Figure 4, left). A B-spline fit is then performed to merge the BSC estimations from the two probes.[15] Han et al.[15] introduced the Polydisperse II model to perform BSC parametrization in dense scattering media, such as biological tissues. This model assumes a Γ (Schulz) scatterer size distribution and uses the fluid-filled sphere model as a form factor.[4] The mean effective radius a, the Schulz width factor z (somewhat the distribution sharpness) and the volume fraction ϕ are the three parameters of the Polydisperse II model. The inversion procedure was performed using the Matlab function *fminsearchbnd* by minimizing the squared error between the experimental data and the expected model with the following constraints: $(a, z) \in [0.1\ \mu m, 100\ \mu m] \times [1, 100]$ and $\phi = 0.70$. Different seed values for a and z were tested.

2.5.2 Ultrasound Envelope Statistics (ES)

The absolute value of the Hilbert transform of the raw RF signals corresponds to the signal envelope. One can fit the Probability Density Function (PDF) of the measured envelope with models to extract ultrasound-based parameters. Indeed, the envelope shape and attributes represent tissue intrinsic properties.[16] In this study, the PDF of each ROI has been fitted to a Nakagami and a Homodyned-K distribution. The scaling parameters Ω from the Nakagami distribution were obtained using a maximum-likelihood estimator. Ω is equivalent to the signal intensity. The effective number of scatterers per resolution cell can be reflected through the parameter μ. This parameter and the ratio of the coherent to the diffuse signal κ from the Homodyned-K distribution were obtained using the XU estimator.[17] The ratio κ can describe the degree of structure in the considered ROI. Further details about each PDF and their related parameters can be found here.[16] The estimates Ω, μ and κ can be corrected for attenuation and diffraction effects as suggested in Mamou et al.[16] (Eq. 9 and 10). The correction then allows the comparisons between the ultrasound-based parameters from ROI located at different positions. In this study, envelope parameters have been extracted from the RF data acquired in the 18 MHz - 38 MHz range.

3. RESULTS

3.1 Optics

Figure 3 (left) shows the results of EBS. The experimental reflectance profile has a good agreement with the fitted model based on the Whittle-Matérn model ($\mathbf{R^2} = 0.98$). The extracted parameters are $L_n = 505\,\mu m$, $A_n = 6.1 \times 10^{-8}$ and $D = 2.03$. Figure 3 (right) shows the experimental differential polarization signal $\Delta I(\lambda)$.

3.2 Ultrasound

Figure 4 (left) shows the results of the BSC parametrization with the Polydisperse II model ($\mathbf{R^2} = 0.96$). The extracted parameters are $a = 9.2\,\mu m$ and $z = 28$. The nucleus and the cell radius distributions extracted from the histological analysis are plotted with the scatterer size distribution extracted from Polydisperse II. The estimated cell radius distribution from histological analysis is in good agreement with the fitted Schulz distribution ($a = 4.6\,\mu m$, $z = 26$, $R^2 = 0.99$). The mean nucleus radius is $a = 2.4\,\mu m$ with a standard deviation $\sigma_a = 0.6\,\mu m$. These results are summarized in Figure 5. Figure 4 (right) shows an example of Homodyned-K and Nakagami fits for one ROI. The mean scale parameter over the 23 ROI is $\Omega = 1.0 \times 10^5$ with a standard deviation equals to 0.6×10^5. The mean corrected scatterer clustering parameter $\mu = 0.13$ and its standard deviation equals 0.6. Finally, the mean coherent to diffuse signal ratio κ equals 0.31 and its standard deviation 0.20.

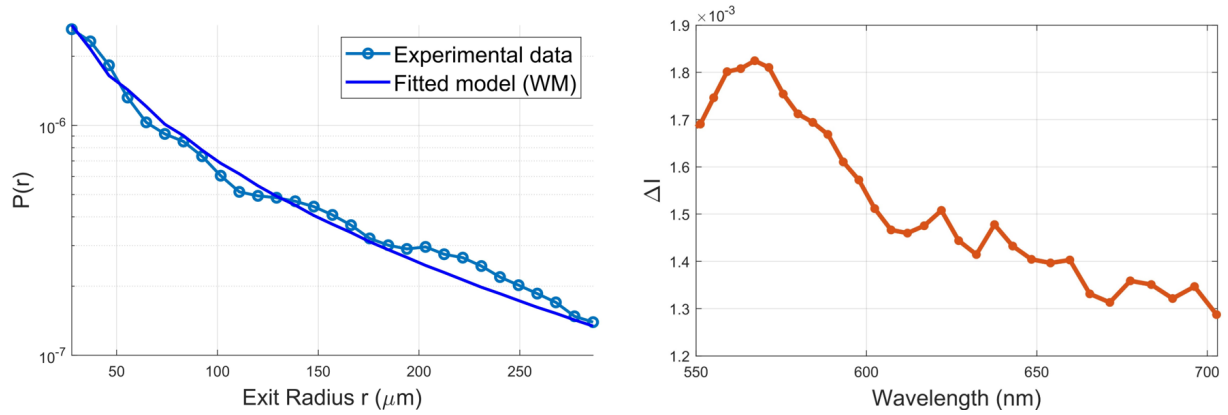

Figure 3. Enhanced Bacskcattering Spectroscopy (left): experimental reflectance profile (a.u.) and corresponding fit as a function of exit radius ($R^2 = 0.98$). Light Scattering Spectroscopy (right): Experimental differential polarization signal (a.u.) versus wavelength

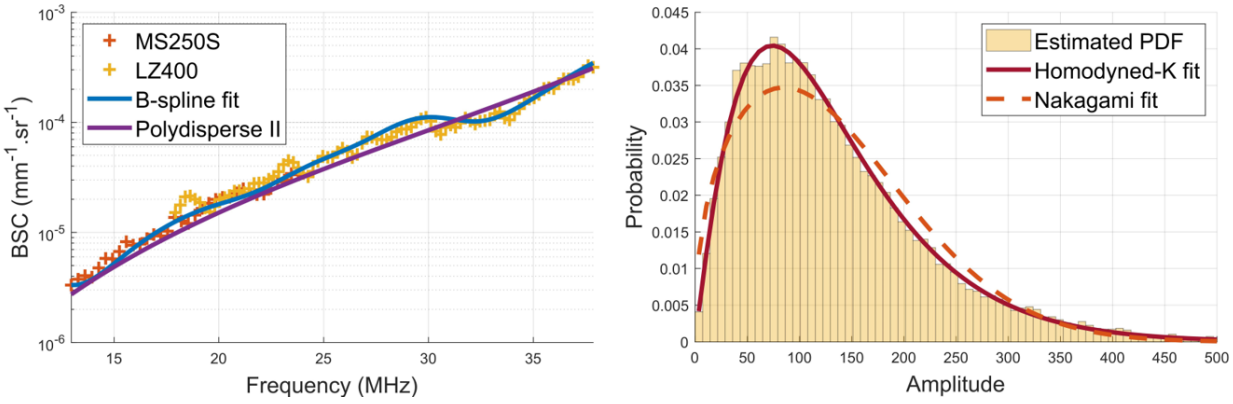

Figure 4. Left: experimental ultrasound backscatter coefficient, resulting B-spline fit and the corresponding fitted Polydisperse II model ($R^2 = 0.96$). Right: Example of an estimated PDF from a single ROI, its Homodyned-K fit ($R^2 = 0.99$) and its Nakagami fit ($R^2 = 0.96$)

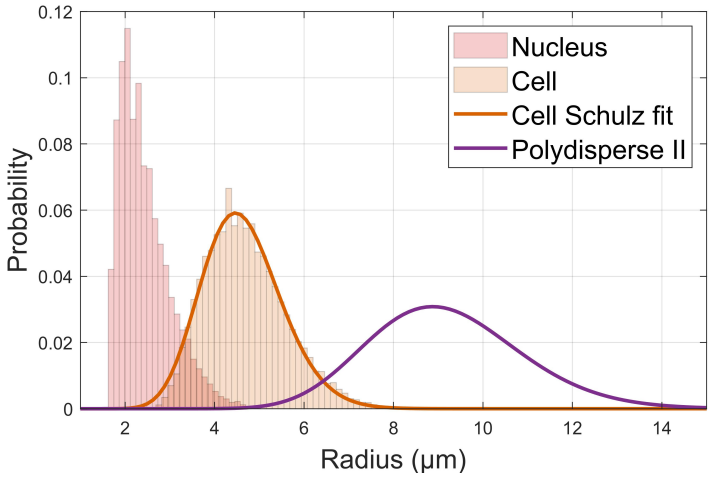

Figure 5. Size distribution estimations performed on histological slices with the estimated distribution from Polydisperse II

4. DISCUSSION

The Whittle-Matérn-based model properly fits the experimental reflectance profile. The parameter L_n can be interpreted physically while the unitless parameters A_n and D have a limited physical meaning outside of the Whittle–Matérn model functional form.[6] However, a representation of the continuous random medium which reflects the spatial refractive index variations can be obtained from this set of parameters.[6] Because the direct measurement of the refractive index variations at the cell scale is technically not possible so far, the extracted Whittle-Matérn parameters cannot be compared with reference values. Nonetheless, relative comparisons of the estimated parameters from different biological samples are possible.[6] Consequently, EBS and the use of the Whittle-Matérn model are more suitable for tissue classification purposes. The LSS fitted model is not shown in this study because the inversion procedure is under investigation.

The same conclusion can be drawn from the ES. The parameter μ can measure the effective number of scatterer per resolution cell to a certain extent,[16] but this correlation is not no longer established when a small number of independent samples are available in a concentrated media.[18] Because of the limited physical interpretations of the absolute values of envelope parameters, one can choose to discriminate certain pathological conditions from others by focusing on their relative values.[3]

Finally, the Polydisperse II fit is in good agreement with the experimental BSC. However, the extracted scatterer size distribution overestimates the histological ground truths and the distribution width. Thus, it not easy to identify the scattering structure. One should note that the fixed volume fraction value set during the inversion procedure is meant to reflect the hypothetic cell volume fraction. A similar approach has been carried out by Han et al.[15] . The BSC parametrization could also be performed with a linear model to further exploit this spectral quantity. This approach extracts the Lizzi-Feleppa (LF) parameters: the slope, the intercept and the midband.[19] Once again, the analysis of these parameters can lead to tissue classification.

5. CONCLUSION

In this study, the ultrasound extracted parameters associated with a physical meaning did not match the histological analyses. However, other light-based and ultrasound-based parameters introduced by the mathematical formalism of well-fitted models could bring relevant contributions for tissue classification in studies involving samples with different pathological conditions for instance.

ACKNOWLEDGMENTS

These works were funded the LABEX PRIMES (ANR-11-LABX-0063) of Université de Lyon, within the program Investissements d'Avenir (ANR-11-IDEX-0007) operated by the French National Research Agency (ANR) and

Infrastructures d'Avenir en Biologie Santé France Life Imaging (ANR-11-INBS-0006). This work was done on the PILoT facility (PILoT, INSA LYON, Bat. L. de Vinci, 7 Av. Jean Capelle 69621 Villeurbanne).

REFERENCES

[1] Radosevich, A. J., Mutyal, N. N., Turzhitsky, V., Rogers, J. D., Yi, J., Taflove, A., and Backman, V., "Measurement of the spatial backscattering impulse-response at short length scales with polarized enhanced backscattering," *Optics letters* **36**(24), 4737–4739 (2011).

[2] Qiu, L., Chuttani, R., Pleskow, D. K., Turzhitsky, V., Khan, U., Zakharov, Y. N., Zhang, L., Berzin, T. M., Yee, E. U., Sawhney, M. S., et al., "Multispectral light scattering endoscopic imaging of esophageal precancer," *Light: Science & Applications* **7**(4), 17174–17174 (2018).

[3] Oelze, M. L., "Quantitative ultrasound techniques and improvements to diagnostic ultrasonic imaging," in [*2012 IEEE International Ultrasonics Symposium*], 232–239 (2012).

[4] Muleki-Seya, P., Guillermin, R., Guglielmi, J., Chen, J., Pourcher, T., Konofagou, E., and Franceschini, E., "High-frequency quantitative ultrasound spectroscopy of excised canine livers and mouse tumors using the structure factor model," *IEEE Transactions on Ultrasonics, Ferroelectrics, and Frequency Control* **63**(9), 1335–1350 (2016).

[5] Turzhitsky, V., Rogers, J. D., Mutyal, N. N., Roy, H. K., and Backman, V., "Characterization of light transport in scattering media at subdiffusion length scales with low-coherence enhanced backscattering," *IEEE Journal of Selected Topics in Quantum Electronics* **16**(3), 619–626 (2009).

[6] Radosevich, A. J., Eshein, A., Backman, V., et al., "Subdiffusion reflectance spectroscopy to measure tissue ultrastructure and microvasculature: model and inverse algorithm," *Journal of biomedical optics* **20**(9), 097002 (2015).

[7] Radosevich, A. J., Rogers, J. D., Turzhitsky, V., Mutyal, N. N., Yi, J., Roy, H. K., and Backman, V., "Polarized enhanced backscattering spectroscopy for characterization of biological tissues at subdiffusion length scales," *Ieee Journal of Selected Topics in Quantum Electronics* **18**(4), 1313–1325 (2011).

[8] Malinet, C., Montcel, B., Dutour, A., Liebgott, H., and Muleki-Seya, P., "Combined ultrasound and light backscattering spectroscopy for cancer characterization: a proof of concept," in [*2022 IEEE International Ultrasonics Symposium (IUS)*], 1–4 (2022).

[9] Rogers, J. D., Radosevich, A. J., Yi, J., and Backman, V., "Modeling light scattering in tissue as continuous random media using a versatile refractive index correlation function," *IEEE Journal of Selected Topics in Quantum Electronics* **20**(2), 173–186 (2013).

[10] Liu, Y., Kim, Y. L., Wali, R. K., Roy, H. K., Goldberg, M. J., Kromine, A. K., Chen, K., and Backman, V., "Simultaneous measurement of angular and spectral properties of light scattering for early cancer detection," in [*Conference on Lasers and Electro-Optics*], CMG4, Optical Society of America (2003).

[11] Fang, H., Ollero, M., Vitkin, E., Kimerer, L. M., Cipolloni, P., Zaman, M. M., Freedman, S. D., Bigio, I. J., Itzkan, I., Hanlon, E. B., et al., "Noninvasive sizing of subcellular organelles with light scattering spectroscopy," *IEEE Journal of selected topics in quantum electronics* **9**(2), 267–276 (2003).

[12] Madsen, E. L., Dong, F., Frank, G. R., Garra, B. S., Wear, K. A., Wilson, T., Zagzebski, J. A., Miller, H. L., Shung, K. K., Wang, S., et al., "Interlaboratory comparison of ultrasonic backscatter, attenuation, and speed measurements.," *Journal of ultrasound in medicine* **18**(9), 615–631 (1999).

[13] Oelze, M. L. and Mamou, J., "Review of quantitative ultrasound: Envelope statistics and backscatter coefficient imaging and contributions to diagnostic ultrasound," *IEEE transactions on ultrasonics, ferroelectrics, and frequency control* **63**(2), 336–351 (2016).

[14] Yao, L. X., Zagzebski, J. A., and Madsen, E. L., "Backscatter coefficient measurements using a reference phantom to extract depth-dependent instrumentation factors," *Ultrasonic imaging* **12**(1), 58–70 (1990).

[15] Han, A. and O'brien, W. D., "Structure function for high-concentration biophantoms of polydisperse scatterer sizes," *IEEE transactions on ultrasonics, ferroelectrics, and frequency control* **62**(2), 303–318 (2015).

[16] Mamou, J., Coron, A., Oelze, M. L., Saegusa-Beecroft, E., Hata, M., Lee, P., Machi, J., Yanagihara, E., Laugier, P., and Feleppa, E. J., "Three-dimensional high-frequency backscatter and envelope quantification of cancerous human lymph nodes," *Ultrasound in medicine & biology* **37**(3), 345–357 (2011).

[17] Destrempes, F., Porée, J., and Cloutier, G., "Estimation method of the homodyned k-distribution based on the mean intensity and two log-moments," *SIAM journal on imaging sciences* **6**(3), 1499–1530 (2013).

[18] Cristea, A., Collier, N., Franceschini, E., Mamou, J., Cachard, C., and Basset, O., "Quantitative assessment of media concentration using the homodyned k distribution," *Ultrasonics* **101**, 105986 (2020).

[19] Muleki-Seya, P., Han, A., Andre, M. P., Erdman Jr, J. W., and O'Brien Jr, W. D., "Analysis of two quantitative ultrasound approaches," *Ultrasonic imaging* **40**(2), 84–96 (2018).